Cyclic Behavior of Component Model of Composite Beam Subjected to Fully Reversed Cyclic Loading

著者	Atsushi Suzuki, Yoshihiro Kimura
journal or publication title	Journal of Structural Engineering
volume	145
number	4
page range	04019015
year	2019-02-15
URL	http://hdl.handle.net/10097/00128417

doi: 10.1061/(ASCE)ST.1943-541X.0002294

CYCLIC BEHAVIOR OF COMPONENT MODEL OF COMPOSITE BEAM SUBJECTED TO FULLY REVERSED CYCLIC LOADING

Atsushi Suzuki [a] and Yoshihiro Kimura [b]

[a] *Ph.D. Candidate, Graduate School of Engineering, Tohoku University, 6-6-11-1215, Aoba, Aramaki, Aoba Ward, Sendai City, Miyagi Prefecture, 980-8565, Japan*

[b] *Professor, New Industry Creation Hatchery Center, Tohoku University, 6-6-11-1216, Aoba, Aramaki, Aoba Ward, Sendai City, Miyagi Prefecture, 980-8565, Japan*

ABSTRACT

In the design of steel structures, composite effects by stud shear connectors are generally measured using ordinary push-out tests. Furthermore, based on those results, the evaluation formulae of the ultimate shear strength are constructed in the design guidelines. However, a concrete slab is subjected to reversed stress during an earthquake, whereas existing tests consider only compressive stresses on the concrete. The mechanical behavior in existing structures thereby might be different from those under compressive force alone.

This research therefore proposes a component model in composite beam modeling the stress in actual buildings. Furthermore, cyclic loading tests are conducted on 14 specimens with different specifications of the stud shear connector, concrete, and rebar. In conclusion, results show that the ultimate shear strength is considerably lower than that under compressive stress. Consequently, this report presents equations to assess structural performance precisely considering various influential factors of composite structures.

*Corresponding Author: Suzuki Atsushi
Tel: +81-90-2791-7316, E-mail: a.suzuki.gsics.tohoku@gmail.com

KEYWORDS

Composite beam; Concrete slab; Cyclic loading test; Headed stud; Ultimate shear strength

INTRODUCTION

In a composite beam, headed studs are widely used to connect the steel beam and concrete slab. This hybrid system incorporates two materials (steel and concrete), which enable structural engineers to realize stiff structures economically. Furthermore, the concrete slab works as restraint against buckling instability. Consequently, an adequate understanding of structural performance is a critical issue to estimate the transfer of shear force between the concrete slab and a steel beam. In addition, the concrete slab is considered as a contributor to enhance the section performance by virtue of the additional reaction force from the concrete under the positive bending and the longitudinal bars under the negative bending in the current design codes (AISC, 2016; Eurocode 4, 2004; AIJ, 2010). However, the abovementioned enhancement is expected based on the presumption that the steel beam and concrete slab demonstrate the designed composite effect even in the ultimate state. Hence, a precise investigation of the mechanical behavior of the stud shear connectors and concrete slab is significantly important to transfer the shear force between the concrete slab and a steel beam.

The framework for the prediction of the ultimate shear strength of stud shear connectors was first constructed by Ollgaard et al. (1971). Specimens of 15 types with several stud arrangements and compressive strength of concrete were selected for push-out tests. The outstanding achievement in this study is the elucidation of evaluation parameter, $\sqrt{F_c E_c}$, where F_c represents the concrete compressive strength and E_c denotes the modulus of elasticity of concrete. Currently, this index is widely accepted in design codes such as the AISC specification (2016), Eurocode 4 (2004), GB 50017-2003 (2004), and the AIJ design recommendation (2010a).

Hawkins and Mitchell (1984) reported the experimentally obtained results on the component model in composite beam under fully reversed cyclic loading. In the experimental series, four failure modes were confirmed in the metal deck stud shear connections: 1) stud shearing, 2) concrete pullout, 3) rib-shearing, and 4) rib punching. Connections with stud shear failures exhibited ductile behavior with stable hysteresis loops. Furthermore, the ultimate shear strengths with stud shear failure and concrete pullout under the reversed cyclic loading are lower, respectively, by approximately 83% and 71% of that under monotonic strength.

Oehlers (1990) constructed a new experimental test to elaborate the performance of headed stud connectors under high-cyclic low-amplitude loading. The loading test results clarified that the strength of stud shear connectors decreases at all cycles of fatigue loading. The stud performance under high-cyclic loadings deteriorates compared with that under monotonic loading. Consequently, Oehlers (1990) newly derived the accumulated damage law to assess the ultimate strength fatigue life.

Gattesco and Giuriani (1996) conducted positively cyclic loading tests modeling the long span beam subjected to repeated loading beyond the elastic range. In the experiment, the residual slip of the stud caused a negative shear force when the composite beam is unloaded. Consequently, it was concluded that the standard push-out test includes limits and modeling inaccuracies that lead to incorrect evaluation of fatigue life. Moreover, the stud accumulated the residual slip up to the overall failure, although the experiment examined mainly one-side cyclic loading.

Bursi and Gramola (1999) further advanced the experimental investigation of the cyclic behavior of headed stud shear connectors under low-cyclic high-amplitude displacements. The experimentally obtained results of 11 specimens under different loading protocols presented that the ultimate shear strength and ductility under the reversed cyclic loading severely degrade compared with those under monotonic loading irrespective of the boundary condition of the concrete slab. Additionally, results show that evaluation formulae in the AISC specification (2016) and Eurocode 4 (2004) overestimate the actual strength of stud shear connectors because they are calibrated upon the monotonic loading tests. Therefore, Bursi and Gramola (1999) concluded that the prevailing guidelines are inadequate, particularly when the reversed displacements govern the stud shear connector response.

Civjan and Singh (2003) presented experimentally obtained results of the modified push-out specimens with different loading protocols, strength of concrete, effects of testing weld integrity, and stud gun versus stick welding installation. The results demonstrated a marked reduction in shear stud capacity when specimens are subjected to reversed cyclic loading. Civjan and Singh (2003) further recommended multiplication of a reduction factor of less than or equal to 0.6 by the assessed ultimate shear strength by AISC specification (2016). In the paper, Civjan and Singh (2003) concluded that the design of shear connector requires consideration of the potential degradation of strength in the seismic event.

Xue et al. (2012) performed eight multi-stud and two single-stud push-out tests with various spacing of studs. The single-stud and multi-stud stiffness values are similar. Moreover, the stud spacing is not strongly influential on the specimen shear stiffness. Furthermore, the ultimate strength per stud of multi-stud specimens is greater by roughly 10% from that of single-stud specimens. In terms of the ductility, the slip at the ultimate shear strength of single-stud specimens is 19% greater than that of multi-stud specimens.

As described above, numerous studies have been conducted on the composite effect of the stud shear connectors. Those findings are used in the prevailing provisions in the field of structural engineering. However, previously reported studies mainly assumed the compressive stress on the concrete slab even if they are subjected to the fully reversed cyclic load. This is presumed to be issued from the difficulty to apply a certain magnitude of tensile stress for the concrete slab because of the geometrical limitation of push-out specimens and the loading apparatus. However, the concrete slab in the moment resisting frame is subjected to tensile stress under the negative bending during earthquakes as illustrated in Fig. 1. Lin et al. (2013, 2014) demonstrated loading tests on composite beams under a negative moment. The collapse mode of composite beams under a negative bending differs considerably from that under a positive bending. This discrepancy implies that the results of ordinary push-out tests are not modeling the actual mechanical stud shear connector behavior. However, Lin et al. (2013, 2014) covered the one side loading only, which can result in the difference of the stress transfer between the concrete slab and the stud shear connector in the fully reversed cyclic loading. Nevertheless, the cyclic behavior and ultimate shear force under the fully reversed cyclic loading has not been ascertained yet.

Based on the discussion above, this research attempts to reveal the ultimate shear strength between stud shear connectors and a concrete slab modeling the stress history of real moment resisting frames during earthquakes. In addition, this research scrutinizes the ultimate shear strength as a mechanical performance defined by the stud shear connectors and the concrete slab since the existing design codes generally adopt the maximum values to calibrate the specification and number of stud shear connectors in the seismic design (AISC, 2016; Eurocode 4, 2004; AIJ, 2010a). For this purpose, this study constructs the component model in a composite beam, which can apply the fully reversed cyclic stress on the stud shear connectors and concrete slab, referring the standard specimen of push-out test guided by Japan Society of Steel Construction (JSSC, 1996). Additionally, this paper carries out a cyclic loading test on the proposed model and attempts to reveal the cyclic behavior of component model, ultimate shear strength, shear resistance mechanism of stud shear connectors, and stress transfer mechanism between the concrete and rebar. Furthermore, the ultimate shear strengths are compared with the current AISC specification and Eurocode 4 to elucidate the applicability of the formulae (AISC, 2016; Eurocode 4, 2004). Finally, this research derives more accurate evaluation formulae than existing guidelines considering the interrelation of the mechanical performance between those under compressive and tensile stresses. The outcome of this research enables structural engineers to adequately secure the prospective composite effect, consequently the section performance of the composite beam.

EXPERIMENT OUTLINE

Outline of specimens

Fig. 2 presents an illustration of the component model for a composite beam. The specimen consists of two H-section steel, headed studs welded with H-section steel, rebar, and a concrete slab. The specimen is symmetrical with the *Z*-axis to examine the behavior specifically for the pure shear force.

The concrete is casted along the *X*-axis to model the practical construction of structures. The specimens are assembled by the bolts and splice plates on the web before they are set up for the loading test.

The pitch of studs and slab thickness are determined in conformity to the recommendation of JSSC (1996). The surface of a jig contacting the concrete is coated with lubricating oil before casting of the concrete to eliminate adhesion and friction.

Fig. 3 depicts the loading frame. The specimen is placed widthwise on the footing beam. External force is applied using a horizontal jack (cap: 1000 kN). Warping of the concrete slab is constrained by steel plates and H-section steel tied by the steel bars.

A list of specimens is presented as Table 1. The 14 specimens have 7 experimental parameters: 1) stud shank diameter (ϕ_{sc}=16 mm, 19 mm, and 22 mm), 2) stud height (h_{sc}=80 mm, 100 mm, and 130 mm), 3) slab width (B=300 mm, 400 mm, and 500 mm), 4) concrete strength (F_c=29.1 N/mm^2, 38.7 N/mm^2, and 64.8 N/mm^2), 5) pitch of rebar (b=200 mm, 400 mm, and 200/400 mm), 6) diameter of rebar (ϕ_{rb}=6 mm, 10 mm, and 13 mm), and 7) loading protocol (fully reversed cyclic, positively cyclic). The rule of designation is presented below Table 1. Rib heights of reinforcing bars are, respectively, 0.6 mm, 0.8 mm, and 1.0 mm in 6 mm, 10 mm, and 13 mm in the rebar diameter. Additionally, the transversal bars are identical with longitudinal bars in all specimens. Regarding the selection of the experimental parameters, it is widely reported that the stud diameter, stud height, slab width, and compressive strength of concrete substantially affect the ultimate shear strength of stud shear connectors in the compressive loading (AISC, 2016; Eurocode 4, 2004; Tagawa et al., 1995). Furthermore, it is expected that the tensile stress is transferred to the rebar as reported by Lin et al.

(2013). Hence, the specification of rebar and its allocation are assumed to be influential for the tension capacity. The specifications of headed stud shear connectors and rebar are selected considering the practical construction and their availability in the market. Additionally, the loading protocol is included as an experimental parameter to clarify the influence of the fully reversed stress on the concrete. In this experimental series, No. 2 is the reference specimen. The rebar arrangements in No. 8, No. 9, and No. 10 are shown in Fig. 4. The strain gauge attachments are given in Fig. 5. In the reference specimen (No. 2), two additional strain gauges are placed on the top and bottom of the stud at x=60 mm.

Loading protocols

The loading amplitude is controlled by the relative displacement between each stud located at Z=120 mm and Z=-120 mm in Fig. 2 (hereinafter designated as stud relative displacement, d). The protocol is gradually increased loading as reversed cyclic loading or positively cyclic loading. The increment is 0.2 mm up to d=1.0 mm and 0.5 mm in over d=1.0 mm in the stud relative displacement. The compressive and tensile stresses are applied, respectively, on the positive and negative side loadings. The specimen is pulled out after the final loading cycle (d=-8.0 mm) is completed.

Material properties

Table 2 shows the mix proportions of concrete. Three mix designs are used with water–cement ratios, W/C of 51.0%, 41.5%, and 35.9%. Table 3 presents the material test results. The material testing of the concrete and steel members are carried out in conformity to JIS A 1108 for the compressive strength test of the concrete, JIS A 1113 for the splitting tensile strength of the concrete, and JIS Z 2241 for the tensile strength test of the steel. The respective compressive strengths are 29.1 N/mm^2, 38.7 N/mm^2, and 64.8 N/mm^2 (Table 3(a)). The yield stress and the ultimate stress of the headed stud are distributed respectively as 351–411 N/mm^2 and 446–486 N/mm^2 (Table 3(b)). The yield stress and the ultimate stress of the steel bar respectively vary from 350–372 N/mm^2 and 493–509 N/mm^2 (Table 3(c)). The yield stress and the ultimate stress of the H-section steel are, respectively, 291 N/mm^2 and 427 N/mm^2 (Table 3(d)). In this experiment, the axial strain of H-section steel does not exceed the yield axial strain in the loading test.

The discrepancy regarding the quality of concrete among specimens are minimized through casting concrete on the same day except No. 13, of which slab is the high strength concrete. Additionally, the headed stud shear connectors, H-section steel, rebar are selected from same lots in the factory. Therefore, the difference of mechanical performance among the specimens is expected to be mainly caused by the experimental parameters.

Curing conditions

The specimens are demolded at the seventh day from the concrete cast. The curing condition is air curing up to the day of loading test. The cylinder specimens of the material test are cured in the same room to give the same temperature history.

RESULTS OF CYCLIC LOADING TESTS ON A COMPONENT MODEL

Cyclic behavior of the component model in the composite beam

In this chapter, the cyclic behavior and ultimate shear strength of component model in the composite beam are scrutinized based on the results of cyclic loading tests. Figs. 6(a)–6(n) portray the hysteresis loops of the respective specimens. The specimens draw the pinching hysteresis loop in larger stud relative displacement except for No. 1 (Fig. 6(a)), which is subjected to positively cyclic loading. Overall, the specimens give larger ultimate shear strengths in positive side loading than those on the negative side loading. The ultimate strength in the negative side remains 27% (No. 11) to 49% (No. 3) of that in the positive side because the cracks originate in the slab under the tensile stress and the concrete loses strength during negative side loading. The largest ultimate shear strengths in both positive and negative sides are obtained in No. 13 (Fig. 6(m)), for which the slab is high strength concrete (F_c=65 N/mm^2). Furthermore, it should be noted that the shear strength under the tensile stress deteriorate rapidly especially in No. 2, No. 6, No.7, No. 9, No. 10, and No. 11 in contrary to that under the positive side loading. This immediate degradation implies the rapid loss of the composite effect between the steel beam and the concrete slab under the negative bending, even though the current design provisions do not differentiate the capacity of stud shear connectors depending on the stress condition in each bending deformation (AISC, 2016; Eurocode 4, 2004; AIJ, 2010a). Therefore, the mechanical performance under the tension loading needs to be scrutinized to secure the composite effect in the structural design.

Figs. 7(a), 7(b) and 7(c) respectively portray the fracture processes of No. 2 at d=0 mm, -4.0 mm and -8.0 mm. Cracks occur at the slab center and embedded position of the studs. Fig. 7 shows that the crack width expands gradually with increased in the stud relative displacement.

Figs. 8(a) and 8(b) respectively present the distribution of bending strain of stud in the positive side and negative side loadings. The horizontal axis is the position along the stud shear connector. The bending strain is calculated by dividing the remainder of strains at the upper and lower side of the stud by 2 as presented in Fig. 5(a). Furthermore, the position of the rebar and the yield bending strain $\varepsilon_{y,sc}$ are also depicted in Fig. 8. In Fig. 8(a), the bending strain of the stud reverses at around x=35 mm. This double curvature originates from the constraint of the horizontal and rotational movement at the head of the stud. In addition, the bending strain near the welded part (x=15 mm) exceeds the yield bending strain at d=1.0 mm. The bending strain of the stud in the negative side loading portrayed in Fig. 8(b) is much smaller than that in the positive side loading. This magnitude relation is the same as the hysteresis loop portrayed in Fig. 6(b).

The loading protocol influence on the cyclic behavior and ultimate shear strength can be refined based on the results of No. 1 (Fig. 6(a)) and No. 2 (Fig. 6(b)). In Fig. 6(a), the component model, which is subjected to the positively cyclic loading, shows no pinching hysteresis. The ultimate shear strength in the positive side in No. 2, which is under the fully reversed cyclic loading, is 371 kN, whereas No. 1 gives 436 kN in the ultimate state. This deterioration originated by the loading protocol is inferred as starting from the crack of concrete occurring in the negative side. It decreased the normal force in the following positive side loading. The mechanism of degradation is presented in Figs. 9(a), 9(b), and 9(c). In the first positive side loading, the stud shear connector receives normal force $N_{s,f}$ from the concrete near the welded part and the headed part (Fig. 9(a)), although the opposite direction of normal force, $N_{s,b}$, supports the stud at the headed part. In the following negative side loading, the concrete originates the cracks and gradually loses its tensile strength (Fig.

9(b)). Therefore, the rebar located on the back side and front side carries normal forces $N_{r,b}$ and $N_{r,f}$, respectively, during loading. The stud shear connectors once again attach the concrete and take normal force $N_{s,f}$ as well as the first cycle in the following positive side loading (Fig. 9(c)). However, less of a contribution of the concrete slab might be taken because of the residual damage under the tensile stress in the previous loading. Therefore, the ultimate shear strength of the component model is affected strongly, even on the positive side. Specimens under the positively cyclic loading do not show cracks at the embedded position of stud, so the performance does not degrade as much as that under fully reversed cyclic loading. The ultimate strength of No. 1 is accomplished at d=5.5 mm, which is larger than that in No. 2 (Fig. 5(b)). However, the stud shear connectors are not classified as ductile in Eurocode 4 (2004) because the characteristic slip capacity does not exceed 6.0 mm. Moreover, the slip performance of component model in this research is lower than that of the ordinary push-out specimens, which usually reach the ultimate shear strength at 30% of the stud diameter (JSCE, 2014). Civjan and Singh (2003) reported that the structural performance of stud shear connectors decreases considerably under cyclic loading. The component models in this research also give the degradation of slip capacity, as Civjan and Singh (2003) demonstrated in earlier experiments. The hysteresis curves of No. 1 and No. 2 are almost identical in the small loading amplitude under the compressive stress, although the slab in No. 2 is subjected to tensile stress in the negative side loading, which indicates that the relation between the shear force and stud slip displacement in the positive side does not differ even under the different loading protocol up to d=1.5 mm (6.8% of the stud diameter). This fact proves that the influence of concrete damage on the shear force in the positive side is not prominent at small loading amplitudes, although it is indispensable in the ultimate state. The previously described discussion proves the necessity of incorporating the interrelation of the mechanical behavior in the positive and negative sides in the evaluation process.

In terms of the stud shank diameter, the ultimate shear strength in the positive side enlarges in the larger stud diameter (Figs. 6(b)–6(d)). The following reasons are inferred: 1) the increase of the stud stiffness gives greater stress transfer to the slab and 2) the wider aspect area carries larger normal force to the slab. The ultimate shear forces in the positive side are 225 kN in No. 3 (ϕ_{sc}=16 mm), 293 kN in No. 4 (ϕ_{sc}=19 mm), and 371 kN in No. 2 (ϕ_{sc}=22 mm). It can be stated that the ultimate shear strength is positively proportional to the stud shank diameter on the positive side. Moreover, the stud relative displacement at the ultimate shear strength increases in a smaller stud diameter. Presumably, the concrete damage does not become severe because the stud absorbs the deformation at the same loading amplitude. However, the ultimate shear forces in the negative side loading shows no specific trend unlike those in the positive side. Additionally, the ultimate shear strengths of No. 2, No. 3, and No. 4 do not differ drastically. Since the studs possess greater stiffness and strength than the slab under the tensile stress, the slab specifications become the dominant factor for the structural capacity. The ultimate strengths are thereby almost identical irrespective of the shank diameter of studs in the negative side.

Regarding the stud height, the ultimate shear strength increases with greater stud height (Figs. 6(b), 6(e), 6(f)). In Fig. 6(e), the slab is shown to fracture at d=-4.4 mm: it loses shear strength. In Fig. 6(f), the shear strength of No. 6 decreases until Q=227 kN and -44 kN, which are much smaller values than No. 2, in the final loading cycle. The curvature in the same stud relative displacement becomes larger in the short stud, which brings huge local stress to the slab. In addition, the height of stud in No. 2 is the same to embedded position of rebar placing back side of slab. Therefore, the longer stud (No. 2) smoothly transfers the stress to the rebar, contrary to No. 5 and No. 6. The ductility thereby differs within the same stud shank diameter. However, the ultimate strengths in the negative side are still almost identical, irrespective of the stud height. In addition, the stud relative displacement at the ultimate shear strength remains at -3.9 mm to -4.4 mm among No. 2, No. 5, and No. 6.

The slab width influence can be understood by Figs. 6(b), 6(g), and 6(h). The ultimate shear strength in the positive side is considerably lower in No. 7 (Fig. 6(g)), with 300 mm slab width, whereas the discrepancy of the ultimate shear strength in the positive side does not appear when the slab width is greater than 400 mm (Figs. 6(b) and 6(h)). However, the stud relative displacement at the ultimate shear strength increases slightly with slab width. A similar trend in the ordinary push-out test was reported from earlier research (Tagawa et al., 1995). Tagawa et al. (1995) concluded that the slab width influence on the mechanical properties of stud shear connectors almost vanishes if the slab has width greater than or equal to 400 mm. The ultimate shear strength in the negative side exhibits a moderate positive relation with the slab width. This enhancement is assumed to derive from the larger cross sectional area of the concrete slab.

In terms of the pitch and number of rebar, Figs. 6(h), 6(i) and 6(j) depict a difference of the performance in each specimen. The largest ultimate shear strength in the negative side loading is obtained in No. 10 (Fig. 6(j)), with 16 rebar in total. However, the enlargement of No. 10 is only 7% in the positive side and 6% in the negative side from No. 8, whereas the total cross sectional area of rebar has doubled, which suggests that the outer rebars do not contribute to the ultimate shear strength as much as their expected yield axial strength. Figs. 10(a), 10(b), and 10(c) depict the stress distribution of rebar embedded in the concrete slab under the negative side loading in No. 10. The rate of axial force to the yield axial strength is also shown in the schematic diagrams. The rebar bears little axial force at d=-1.0 mm, when the crack on the concrete slab is still not detected by the strain gauges or visual inspection (Fig. 10(a)). In the ultimate state, the rebar near the headed studs reaches the yield strength, besides the outer rebar remains in the elastic region (Fig. 10(b)). The axial force of the front outer rebar is roughly 50% of their yield axial force at d=-2.5 mm when the specimen carries the ultimate shear strength in the negative side. Consequently, the contribution of the outer rebar on the structural capacity might be estimated as approximately 50% of the inner rebar. Even in the larger stud relative displacement, the axial force of outer rebar is not increased drastically: it remains in the elastic stage (Fig. 10(c)).

The influence of the rebar diameter is visible from No. 2, No. 11, and No. 12 (Figs. 6(b), 6(k), and 6(l)). The largest ultimate shear strength in the positive side loading in No. 2 becomes slightly larger than that in No. 12, whereas No. 12 has the largest ultimate shear strength in the negative side loading. It might be inferred that the specimen with higher gauge rebar has greater shear strength. However, the opposite result is demonstrated between No. 2 and No. 12. The reversal of the ultimate shear strength in positive side between No. 2 and No. 12 is explainable through the concrete damage in negative side loading. In Fig. 6(l), No. 12, for which rebar has 13 mm diameter, resists greater shear force in the negative side, even with a small loading amplitude. However, a wide crack suddenly appears to release the larger fracture energy at d=-1.3 mm. Consequently, comparatively little stress in the positive side is carried to the concrete slab even in the positive side loading. The ultimate strength in the positive side thereby degrades even with larger cross sectional area of rebar. In No. 11, for which the rebar diameter is only 6 mm, the ultimate shear force is markedly lower on the negative side. ACI (2003) reported that the majority of stress transfer between the concrete and the reinforcing bars is demonstrated by the bearing of ribs. Furthermore, the other contributors (adhesion and friction) gradually diminish with increase in the slip at the interface. The rib height of reinforcing bars with 6 mm in the rebar diameter is the smallest in the experimental series, resulting in the rapid degradation of bond strength between the rebar and concrete. Therefore, the ultimate shear strength and ductility of No. 11 becomes much less than those of other specimens.

The concrete strength is the most crucially important factor affecting shear strength in this experimental series. In Figs. 6(b) and 6(m), the ultimate shear force of No. 13, with concrete strength of 65 N/mm^2, has 491 kN in the positive side and -235 kN in the negative side, whereas those in No. 2 are, respectively, only 371 kN (76%) and -120 kN (51%). Enhancement of the ultimate shear strength issued from the high compressive strength of concrete is widely described in earlier reports of the relevant literature (e.g., Ollgaard et al., 1971; Li and Cederwall 1996; Luo et al., 2016). Regarding the enlargement of the ultimate shear strength in the negative side loading, the concrete material gradually loses tensile strength with crack expansion during cyclic loading. Consequently, increase of the tensile strength is not the direct factor to originate larger ultimate shear strength in the tension loading. Rather, it is assumed to be achieved because of larger bond force between rebar and concrete, which enables the stress to be transferred between the stud and rebar during negative side loading.

The effectiveness of rebar is presented clearly in Fig. 6(n). The specimen without reinforcements shows origination of the overall fracture at d=-0.5 mm and immediately loses shear strength, which implies the necessity of the rebar to secure the composite effect between the steel beam and concrete slab, particularly under negative bending. Additionally, the maximum contribution of concrete on the shear force can be ascertained from this result, even though the tensile strength of concrete in No. 14 differs from that of other specimens. The concrete can resist up to -105 kN, which is almost 80%–90% of the ultimate strength of other specimens. Therefore, it can be stated that the concrete and rebar do not carry the load parallel during the loading test. The concrete mainly resists the tensile stress before tension softening caused by the cracks. Furthermore, the rebar inherits the tensile stress in the ultimate states. Consequently, the envelope of hysteresis curve comes to resemble a bi-linear configuration in the summation of two components.

Fig. 11 depicts a comparison of the ultimate shear strength per stud, q_{max}/A_{sa}, between the positive and negative side loadings. Here, q_{max} is the ultimate shear strength of one stud; A_{sa} is the cross sectional area of one stud. The ultimate shear strengths of the respective sides are positively proportional to each other. The ultimate shear strength in the positive side loading relates to the compressive strength of concrete, while that in the negative loading is affected by the bond strength between the concrete and reinforcing bars. It is widely recognized that each strength possesses a positive relationship each other (ACI, 2003; Eurocode 2, 2002, AIJ, 2010b). Hence, it is expected that the ultimate shear strengths in the positive side and negative side demonstrate the positive proportional relationship. The ultimate shear strength in No. 13 therefore locates upper right in Fig. 11. Furthermore, the stud shear connectors with smaller diameter (No. 3 and No. 4) place comparatively on the upper right. As described in the comparison regarding the stud diameter, the compressive stress on the concrete is not localized due to larger flexibility of slender stud shear connectors in the positive loading. In addition, the ultimate shear strength in the negative side loading does not differ drastically depending on the diameter of stud shear connectors. The ultimate shear strength per cross sectional area therefore enlarges in smaller stud diameter. Additionally, in Fig. 11, the specimens with greater number of reinforcing bars (No. 10) or larger diameter of rebar (No. 12) locate relatively on the upper right, whereas those with the coarse arrangement of longitudinal bars (No. 11) place on the lower left. This evinces that the deterioration mechanism portrayed in Fig. 9 governed the ultimate shear strength of the component model in the composite beam. In summation, the positive proportional relation is demonstrated in this experimental series as illustrated in Fig. 11. Furthermore, it should be noted that the ultimate shear strengths in No. 2, No. 7, No.8, No. 9, No. 10, No.11, and No. 12 become identical in the conventional evaluations in AISC specification (2016), Eurocode 4 (2004), GB50017-2003 (2004), and AIJ design recommendation (2010a). However, the ultimate shear strength becomes inconsistent due to the discrepancy of the specification of slab. Fig. 11 therefore proves the significance to harmonize the evaluation of the capacity under loadings in both sides.

Stress transfer mechanism between rebar and concrete of a component model

In this section, the stress transfer mechanism between concrete and rebar in the component model is scrutinized, particularly addressing No. 2: the reference specimen in this experimental series.

Figs. 12(a) and 12(b) depict the relation between the normalized strain of the slab, $\varepsilon_{sl}/\varepsilon_{sl,t}$, and the stud relative displacement. Here, ε_{sl} is the measured strain of slab; $\varepsilon_{sl,t}$ is the ultimate tensile strain of concrete. In the small stud relative displacement, the strain of slab and stud relative displacement represent a linear relation. However, the relation is disturbed gradually. Finally, a crack in the slab originates at d=-2.4 mm.

Figs. 13(a)–13(d) show the relation between the normalized strain, $\varepsilon_{rb}/\varepsilon_{rb,y}$, of rebar and loading amplitude. Here, ε_{rb} is the measured axial strain of rebar; $\varepsilon_{rb,y}$ is the yield axial strain of rebar. Also, (a) is the front side at Z=147.5 mm, (b) is the front side at Z=50 mm, (c) is the back side at Z=147.5 mm, and (d) is the back side at Z=50 mm. Overall, the values increase rapidly at crack origination, which proves that the stress is transferred to the rebar after the concrete loses strength because of the crack. In Fig. 13(a), the axial strain exceeds the yield strain, which is obtained as a quotient of the yield stress of a steel bar and elastic modulus. However, as described in Fig. 13(a), the strain of rebar placed on the front side decreases up to 10-75% of the yield strain in the positive side loading (2 mm $\leq d \leq$ 5 mm), while the strain does not jump into the compressive side once the stress is transfer to the rebar due to the concrete crack. Moreover, the strain of rebar near the slab center retains only 10%–25% of the yield strain in the positive side loading, as presented in Fig. 13(b). However, the strain increases gradually up to 75% of the yield strain in the negative side loading. Therefore, it can be concluded that the shear strength in the positive side relies mainly on the concrete, whereas the rebar on the front side hugely contributes to the shear strength in the negative side. The strain of rebar in the back side of slab shows different behavior from that shown in Figs. 13(a) and 13(b). The strain remains in the elastic region even for the negative side loading, which indicates that the tensile stress is distributed mainly to the rebar on the front side of slab, as shown in Fig. 10 presented in the previous section. In the positive side, the strain tends to increase because of the leverage of the stud, as presented in Fig. 9.

Figs. 14(a) and 14(b) show the slip displacement of the stud s_{sc} and slab, s_{sl}, arranged by the stud relative displacement d. The slip displacement of the stud, s_{sc}, is the distance between the welded position of stud and the front edge of the slab measured by the dial gauge installed at the inner flange (Fig. 3(b)). The slip displacement of the slab, s_{sl}, is the movement of bottom slab measured by the dial gauge placed on the footing beam (Fig. 3(b)). In Fig. 14(a), the slip displacement suddenly decreases because of the crack at d=-2.4 mm. The slip displacement has a linear relation with the stud relative displacement before the crack origination. The magnitude in the negative side does not exceed -2.0 mm, even in the final loading cycle, because the slab moves with the stud after the concrete loses the strength because of the crack. In addition, the slip displacement shifts gradually to the positive side at d=0 mm because the concrete edge displacement does not return back to the origin, which implies that concrete does not brace the stud in the negative side loading, which makes the bending strain of stud smaller in Fig. 8(b). In Fig. 14(b), the slip displacement of slab stays below 1.0 mm in the negative side because the stud does not strongly pull the slab after the concrete loses the tensile strength.

COMPARISON WITH PREVAILING DESIGN CODES

Comparison with evaluation formula in AISC

AISC determines the ultimate shear strength of one headed stud anchor, q_{max}, embedded in a solid concrete slab by Eq. (1) (AISC, 2016).

$$q_{max} = 0.5A_{sc}\sqrt{F_c E_c} \le R_g R_p A_{sc} F_u \quad (1)$$

In that equation, F_u stands for the specified minimum tensile strength of a steel headed stud anchor. In the component model in this research, R_g and R_p can be given as 1.0 and 0.75 because the headed studs are welded directly to the steel shape (AISC, 2016).

Figs. 15(a) and 15(b) show comparisons between experimentally obtained results and evaluation equation in AISC specification (AISC, 2016). The horizontal axis is the square root of the product of F_c and E_c. The vertical axis is the quotient of shear strength per stud and cross-sectional area of stud: q_{max}/A_{sc}. In addition, Shimada (2016) constructed the database of previous ordinary push-out tests. The results arranged by Shimada (2016) are also presented respectively in Figs. 15(a) and 15(b) to clarify the difference with the conventional specimens.

In Fig. 15(a), the experimentally obtained results belong to the lower bound of the database. However, all ultimate shear strengths place below the evaluation formula in AISC specification (AISC, 2016), which implies that the guideline of AISC (2016) is not sufficiently conservative in terms of securing the composite effect. Fig. 15(b) presents a comparison of the ultimate shear strength in the negative side loading. Overall, the ultimate shear strength locates much lower than Eq. (1) and the database, which implies that the composite effect under the negative bending is not satisfactory as much as the AISC specification is expecting (AISC, 2016).

Comparison with evaluation formula in Eurocode 4

Eurocode 4 (2004) defines the ultimate shear strength of one headed stud anchor embedded in a solid concrete slab by Eq. (2) and (3).

$$q_{max} = \mathrm{Min}\left(\frac{0.8 F_u \pi {\phi_{sc}}^2 / 4}{\gamma_V}, \frac{0.29 \alpha {\phi_{sc}}^2 \sqrt{F_c E_c}}{\gamma_V} \right) \tag{2}$$

$$\alpha = \begin{cases} 0.2\left(\dfrac{h_{sc}}{\phi_{sc}} + 1 \right) & \left(3 \le h_{sc}/\phi_{sc} \le 4 \right) \\ 1.0 & \left(h_{sc}/\phi_{sc} > 4 \right) \end{cases} \tag{3}$$

Therein, γ_V is the partial factor. Eurocode 4 (2004) recommends 1.25 for the value of γ_V. Actually, the evaluation formula in Eurocode 4 is much more conservative than that in AISC (2016). The ultimate shear strengths determined by concrete crush and stud failure are, respectively, 58% and 85% of Eq. (1). Figs. 16(a) and 16(b) respectively present a comparison between experimentally obtained results and Eurocode 4's equation in the positive side and negative side. Fig. 16(a) shows good agreement except No. 14, which is not reinforced by rebar. In addition, the experimentally obtained results are assessed conservatively except No. 7, which has 300 mm slab width. Therefore, it can be inferred that the ultimate shear strengths in the positive side are roughly evaluated by Eqs. (2) and (3). However, the difference of the ultimate shear strength issued from the specification of rebar diameter and its allocation, which are the influential factors on the tension capacity, is not demonstrated by the evaluation formula. The ultimate shear strengths in the negative side do not exceed those of the formula in Fig. 16(b). The experimental values remain at 24% at minimum (No. 14) and 61% at maximum (No. 3), which proves the necessity to propose the evaluation formula for the ultimate shear strength under the tensile stress.

DERIVATION OF EVALUATION FORMULAE FOR A COMPONENT MODEL IN A COMPOSITE BEAM

In this chapter, the evaluation formulae of the ultimate shear strength in the positive and negative sides are derived to assess the performance accurately.

Eurocode 4 (2004) considers the stud height, h_{sc}, and shank diameter, ϕ_{sc}, ratio as a coefficient, α. However, the value of α becomes a constant, 1, in h_{sc}/ϕ_{sc} > 4, which means that the effect of the aspect ratio of headed stud is neglected. This presumption designates that the ultimate shear strength divided by the cross sectional area is assessed as equal in the same concrete property when stud shear connectors become narrow. However, Figs. 15 and 16 demonstrate that the influence of h_{sc}/ϕ_{sc} should be refined based on the experimentally obtained results. Based on the discussion presented above, this research elaborates the coefficient to define the effect of aspect ratio in the positive side, α^+, referring to the experimentally obtained results. Coefficient α^+ is calculable back by Eq. (4) through solving Eq. (2) for α. Here, q_{max}^+ denotes the ultimate shear strength per stud shear connector on the positive side.

$$\alpha^+ = \frac{\gamma_v q_{max}^+}{0.29\phi_{sc}^2\sqrt{F_c E_c}} \tag{4}$$

The ultimate shear strength in the negative side does not relate directly to the compressive strength of concrete. In addition, the concrete loses its tensile strength in the ultimate state. Therefore, substituting the compressive strength in Eq. (4) by the tensile strength is inadequate for the evaluation. Instead, this research was conducted to employ the bond strength, F_{bd}, between the concrete and rebar. The bond strength of deformed steel bars is determined using Eq. (5) (AIJ, 2010b). Furthermore, the coefficient in the negative side α^- is backward calculable by Eq. (6). Here, q_{max}^- denotes the shear strength per stud shear connector on the negative side.

$$F_{bd} = \mathrm{Min}\left(\frac{1}{10}F_c, \left(1.35 + \frac{1}{25}F_c\right)\right) \tag{5}$$

$$\alpha^- = \frac{\gamma_v q_{max}^-}{0.29\phi_{sc}^2\sqrt{F_{bd}E_c}} \tag{6}$$

Fig. 17 presents the obtained coefficients α^+ and α^- arranged by the stud aspect ratio h_{sc}/ϕ_{sc} in Fig. 17(a) and the inverse of ϕ_{sc}^2 in Fig. 17(b). The displayed specimens in Fig. 17 are No. 2, No. 3, No. 4, No. 5, and No. 6, which possess the same concrete properties and different specifications of studs. In Fig. 17(a), the coefficients exceed Eq. (3) in $h_{sc}/\phi_{sc} > 4$ and the value of coefficient enlarges up to 1.25 in $h_{sc}/\phi_{sc} = 8.1$, which reveals that the guidance of Eurocode 4 (2004) secures conservative assessments in spite of its inaccuracy. Fig. 17(a) clearly portrays that the coefficient in the positive side, α^+, is positively proportional to h_{sc}/ϕ_{sc}. Consequently, the following formula can be derived by the single regression analysis. This study inherits the existing function of Eurocode 4 (2004) in $h_{sc}/d \leq 4$.

$$\alpha^+ = \begin{cases} 0.2\left(\dfrac{h_{sc}}{\phi_{sc}} + 1\right) & \left(3 \leq h_{sc}/\phi_{sc} \leq 4\right) \\ 0.055\left(\dfrac{h_{sc}}{\phi_{sc}} + 14.2\right) & \left(h_{sc}/\phi_{sc} > 4\right) \end{cases} \tag{7}$$

By contrast, the coefficient in the negative side, α^-, is positively proportional to the inverse of ϕ_{sc}^2. This clear relation is given by the consistency of the ultimate shear strength irrespective the specification of stud under tensile stress, as described in this paper. Therefore, assessing α^- by the stud aspect ratio is inadequate because the stud height is not a determinant of the performance in the negative side loading. Additionally, constructing the evaluation formula of α^- employing $1/\phi_{sc}^2$ enables reduction of the stud shank diameter term from Eq. (2). This research thereby proposed the prediction model of α^- as Eq. (8) through single regression analysis. The intercept is intentionally fixed as 0 to make the regression equation pass the origin. However, it has sufficient accuracy.

$$\alpha^- = \frac{550}{\phi_{sc}^{\ 2}} \tag{8}$$

Prediction of the ultimate shear strength in the positive side, $q_{max}^{+\prime}$ (Eva.), and the negative side, $q_{max}^{-\prime}$ (Eva.), might be implemented by substituting Eqs. (7) and (8) in Eq. (2). The ultimate shear strengths in the positive and negative sides are interrelated under the reversed cyclic loading (Fig. 11). For that reason, it is necessary to consider cracks in concrete, which weaken the stress transfer between a stud and concrete. Accordingly, the evaluation formula of the ultimate strength in the negative side is first constructed because it is the critical mechanism in this experimental series. It is readily apparent that the ultimate shear strength in the negative side deeply relates to the rebar allocation and its diameter. In Fig. 10, it has been clarified that the axial force of rebar is not uniform in a cross section of concrete slab. The rebar near the edge of slab has roughly 50% of the yield axial force in No. 10. Consequently, this study defines the following assumption in the evaluation: 1) steel bars arranged with 200 mm pitch contribute 100% of their cross sectional area and 2) steel bars arranged with 400 mm pitch contribute 50% of their cross sectional area. The effective cross sectional area of rebar is calibrated based on the presumption stated above. Fig. 18(a) depicts the correction factor, $\beta^- = q_{max}^-$ (Exp.)/$q_{max}^{-\prime}$ (Eva.), arranged by the yield axial strength of the effective cross sectional area of rebar: $f_{y,ef}$. Here, q_{max}^- (Exp.) is the experimental value in the negative side loading. For simplicity, β^- obtained in No. 2, No. 9, No. 10, No. 11, No. 12, and No. 14 are displayed in Fig. 18(a). Fig. 18(a) shows that the correction factor is generally positively proportional to the effective yield strength of rebar: $f_{y,ef}$ (unit: kN). Therefore, the correction factor is induced through the single regression analysis as

$$\beta^- = 0.002 f_{y,ef} + 0.78 \quad . \tag{9}$$

Consequently, the ultimate shear strength is predicted by Eq. (10) with Eq. (9). In Eq. (10), the term of the stud shank diameter has already been reduced through the derivation process. Fig. 18(b) shows that the proposed formulae precisely evaluate the experimentally obtained results.

$$q_{max}{}^- = \mathrm{Min}\left(\frac{0.8F_u \pi \phi_{sc}{}^2/4}{\gamma_v}, \frac{159.6\beta^- \sqrt{F_{bd} E_c}}{\gamma_v} \right) \tag{10}$$

Finally, the ultimate shear strength in the positive side is calibrated considering the influence of reversed cyclic loading. As Fig. 11 suggests, damage to the concrete slab strongly affects the structural performance in the positive side, particularly in the specimen with low ultimate shear strength in the negative side. Based on the consideration presented above, the correction factor in the positive side, $\beta^+ = q_{max}{}^+$ (Exp.)/ $q_{max}{}^{+\prime}$ (Eva.), is compared with the evaluated ultimate shear strength in the negative side, where $q_{max}{}^+$ (Exp.) and $q_{max}{}^{+\prime}$ (Eva.) respectively represent the experimental and evaluated values in the positive side loading (Fig. 19(a)). Correction factor β^+ is seemingly proportional to the ultimate shear strength in the negative side. Therefore, this research represents an attempt to assess the correction factor as the following function.

$$\beta^+ = 0.0072 q_{max}{}^- (\mathrm{Eva.}) + 0.7706 \tag{11}$$

The ultimate shear strength in the positive side is calculable in Eq. (12) with Eq. (7) and (11).

$$q_{max}^{+} = \mathrm{Min}\left(\frac{0.8 F_u \pi \phi_{sc}^{2} / 4}{\gamma_v}, \frac{0.29 \alpha^{+} \beta^{+} \phi_{sc}^{2} \sqrt{F_c E_c}}{\gamma_v} \right) \tag{12}$$

Fig. 19(b) presents a comparison between the evaluated and experimentally obtained results. The accuracy of prediction is improved compared with Fig. 16(a), although Eurocode 4 (2004) intends to exhibit the conservative assessment. However, proposed formulae of the ultimate shear strength adequately include the influential factor with taking the interrelation between those in the positive and negative side loadings into consideration, which is representing the genuine mechanical behavior of the component model in the composite beam.

In this research, the specimens in the experimental series cover h_{sc}/ϕ_{sc}=3.6 to 8.1 in the stud specification. The applicable scope range of the proposed evaluation formulae is therefore defined within h_{sc}/ϕ_{sc}=3.6 to 8.1.

CONCLUSION

For this study, cyclic loading tests on a component model of a composite beam were demonstrated with several influential factors on the mechanical performance. Based on the experimentally obtained results, the cyclic behavior and stress transfer between the headed stud and concrete slab were refined here. In addition, the applicability of prevailing equations to assess the shear strength of headed stud connectors was investigated in terms of those under compressive and tensile stresses. The remarkable findings are summarized below.

1) The ultimate shear strengths under the tensile stress become 27%–49% of those under the compressive stress. Those under tensile stress do not differ drastically depending on the stud

specifications.

2) The normal force by concrete decreases with crack expansion during cyclic loading. Therefore, the ultimate shear strength degrades when the slab is subjected to fully reversed cyclic loading compared with that under positively cyclic loading.

3) The ultimate strength of the component model in the composite beam places below the evaluation formula (Eq. (1)) in the AISC specification. Particularly, the value in the negative side becomes only 17%–44% of the results predicted in the guideline.

4) The prediction (Eq. (2)) of Eurocode 4 roughly grasps the ultimate shear strength of the composite beam subjected to the fully reversed cyclic loading. However, the ultimate shear strength under the tensile stress becomes much lower than the assessed value of Eurocode 4.

5) The derived equations considering the interrelation between compressive and tensile sides can appropriately predict the ultimate shear strength of the component model in a composite beam.

In the future research, the finite element model will be constructed based on the experimental results in this paper. Furthermore, the comprehensive parametric study will be demonstrated to interpolate and supplement the influential parameters of the experiment. The effective axial strength of rebar and mechanism of bearing force between stud shear connectors and concrete slab will be presented as a continuous function through the calibrated results.

ACKNOWLEDGMENTS

This research was funded by a Grant-in-Aid for JSPS Fellows Grant Number 17J03340 “Establishment of Damage Control Design for Braced Steel Structures Considering Axial Forces Act on Beams" (Principal Investigator: Atsushi Suzuki) and a Grant from The Japan Iron and Steel Federation (Principal Investigator: Atsushi Suzuki).

The experiments were supported by Dr. Sachi Furukawa and Ms. Kanako Abe. We extend our deepest gratitude for their sincere cooperation.

REFERENCES

ACI Committee 408 (2003). "*Bond and Development of Straight Reinforcing Bars in Tension*", American Concrete Institute

AIJ (2010a). "*Design Recommendations for Composite Constructions*," Maruzen Publishing Co. Ltd., 92. (in Japanese)

AIJ (2010b). "*Standard for Structural Calculation of Reinforced Concrete Structures*," Maruzen Publishing Co. Ltd., 7. (in Japanese)

AISC (2016). "*Specification for Structural Steel Buildings*," American Institute of Steel Construction Inc., Chicago, Sect. I8.

Bursi, O. S. and Gramola, G. (1999) "Behaviour of Headed Stud Shear Connectors under Low-cycle High Amplitude Displacements," *Materials and Structures,* 32, 290–297.

Civjan, Scott A. and Singh, Prabhjeet (2003) "Behavior of Shear Studs Subjected to Fully Reversed Cyclic Loading," *Journal of Structural Engineering,* 129, 1466–1474.

Eurocode 2 (2004). "*Design of concrete structures Part 1-1: General rules and rules for buildings*", European Committee for Standardization

Eurocode 4 (2004). "*Design of composite steel and concrete structures Part 1-1: General rules and rules for buildings*", European Committee for Standardization

Gattesco, N. and Giuriani, E. (1996) "Experimental Study of Stud Shear Connectors Subjected to Cyclic Loading," *Journal of Constructional Steel Research*, 38(1), 1–21.

Hawkins, Neil M. and Mitchell, Denis. (1984) "Seismic Response of Composite Shear Connections," *Journal of Structural Engineering*, 110(9), 2120–2136.

JSCE. (2014). "*Standard specifications for hybrid structures 2014*," Maruzen Publishing Co. Ltd. (in Japanese)

JSSC. (1996). "*Guideline of Standard push-out tests of headed stud and current situation of research on studs shear connectors*," Japan Society of Steel Construction. (in Japanese)

Li, An and Cederwall, Krister (1996). "Push-out Tests on Studs in High Strength and Normal Strength Concrete," *Journal of Constructional Steel Research*, 36(1), 15–29, DOI: 10.1016/0143-974X(94)00036-H

Lin, Weiwei, Yoda, Teruhiko, and Tachiguchi Nozomu (2013). "Fatigue Tests on Straight Steel-Concrete Composite Beams Subjected to Hogging Moment", *Journal of Constructional Steel Research*, 80(1), 42-56, DOI: 10.1016/j.jcsr.2012.09.009

Lin, Weiwei, Yoda, Teruhiko, Taniguchi, Nozomu, Kasano Hideyuki, and He Jun (2014). "Mechanical Performance of Steel-Concrete Composite Beams Subjected to a Hogging Moment", *Journal of Structural Engineering*, 140(1), DOI: 10.1061/(ASCE)ST.1943-541X.0000800

Luo, Yunbiao, Hoki, Kazuaki, Hayashi, Kazuhiko, and Nakashima, Masayoshi (2016). "Behavior and Strength of Headed Stud–SFRCC Shear Connection. I Experimental Study." *Journal of Structural Engineering*, 142(2), DOI: 10.1061/(ASCE)ST.1943-541X.0001363

Ministry of Construction of China (2004). "*BG50017-2003: Code for design of steel structures*," Beijing, China Planning Press, 121. (in Chinese)

Oehlers, Deric John. (1990) "Deterioration in Strength of Stud Connectors in Composite Bridge Beams," *Journal of Structural Engineering*, 116, 3417–3431.

Ollgaard, J. G., Slutter, R.G., Fisher, J. W. (1971). "Shear strength of stud connectors in lightweight and normal weight concrete," *AISC Engineering Journal*, 55–64.

Shimada, Yuko et al. (2016). "Consideration of design formula of headed studs," *Proceedings of Constructional Steel*, 24, 103–110. (in Japanese)

Tagawa, Yasuhisa, Hiragi, Hirokazu, Ogata, Motoomi, Inoue, Kazuo, and Matsui, Shigeyuki (1995). "An Investigation on Standard Push-out Test Method for Headed Stud Shear Connectors," *Journal of Steel Construction Engineering*, 2, 47–60. (in Japanese)

Xue, Dongyan, Liu, Yuqing, Yu, Zhen, and He, Jun. (2012) "Static behavior of multi-stud shear connectors for steel–concrete composite bridge," *Journal of Constructional Steel Research*, Vol. 74, 1–7, DOI: 10.1016/j.jcsr.2011.09.017

Figure Captions

Fig 1. Stress History of Concrete Slab: (a) positive bending and (b) negative bending

Fig 2. Component Model in Composite Structure (unit: mm): (a) side view and (b) front view.

Fig. 3. Loading Frame (unit: mm).

Fig. 4. Arrangement of Rebar (unit: mm): (a) No. 8, (b) No. 9, (c) No. 10.

Fig. 5. Attachment of Strain Gauges (unit: mm): (a) stud and jig, (b) rebar, and (c) concrete slab.

Fig. 6. Hysteresis Curves: (a) No. 1, (b) No. 2, (c) No. 3, (d) No. 4, (e) No. 5, (f) No. 6, (g) No. 7, (h) No. 8, (i) No. 9, (j) No. 10, (k) No. 11, (l) No. 12, (m) No. 13, and (n) No. 14.

Fig. 7. Fracture Process: (a) d=0 mm, (b) d=-4.0 mm, and (c) d=-8.0 mm.

Fig. 8. Bending Strain of Stud: (a) positive and (b) negative.

Fig. 9. Influence of Reversed Cyclic Loading: (a) first positive side loading, (b) following negative side loading, and (c) following positive side loading.

Fig. 10. Stress Distribution under Negative Side Loading (No. 10): (a) d=-1.0 mm, (b) d=-2.5 mm (ultimate shear strength), and (c) d=-4.0 mm.

Fig. 11. Comparison of Ultimate Shear Strength of Positive and Negative Sides.

Fig. 12. Strain of Concrete Slab: (a) side (left side, Z=120 mm) and (b) front (left side, Z=120 mm)

Fig. 13. Strain of Rebar: (a) front (left side, Z=147.5 mm), (b) front (left side, Z=50 mm), (c) back (left side, Z=147.5 mm), and (d) back (left side, Z=50 mm).

Fig. 14. Slip Behavior: (a) headed stud and (b) concrete slab.

Fig. 15. Comparison between Experimental Results and AISC's Equation: (a) positive and (b) negative.

Fig. 16. Comparison between Experimental Results and Eurocode-4's Equation: (a) positive and (b) negative.

Fig. 17. Coefficients α^+ and α^- arranged by h_{sc}/ϕ_{sc} and $1/\phi_{sc}^2$: (a) positive and (b) negative.

Fig. 18. Evaluation of the ultimate shear strength in the negative side: (a) reduction factor and (b) comparison.

Fig. 19. Evaluation of Ultimate Shear Strength in Positive Side: (a) correction factor and (b) comparison.

Table Captions

Table 1. List of Specimens

Table 2. Mix Proportion

Table 3. Material Properties: (a) concrete, (b) headed stud, (c) rebar, and (d) H-section steel.

Table 1. List of Specimens

No.	Designation	Headed Stud		Concrete		Rebar		Protocol
		Diameter [mm]	Length [mm]	Width [mm]	Strength [N/mm^2]	Pitch [mm]	Diameter [mm]	
1	22-130-400-29-200-10-P	22	130	400	29	200	10	Positively
2	22-130-400-29-200-10-R							Reversed
3	16-130-400-29-200-10-R	16	130					
4	19-130-400-29-200-10-R	19	130					
5	22-80-400-29-200-10-R	22	80					
6	22-100-400-29-200-10-R		100					
7	22-130-300-29-200-10-R			300				
8	22-130-500-29-200-10-R			500				
9	22-130-500-29-400-10-R					400		
10	22-130-500-29-200/400-10-R					200/400		
11	22-130-400-29-200-6-R			400		200	6	
12	22-130-400-29-200-13-R						13	
13	22-130-400-65-200-10-R				65		10	
14	22-130-400-39-U-R				39	-	-	

22 - 130 - 400 - 29 - 200 - 10 - R

Protocol (R, Reversed cyclic; P, Positively cyclic)

Diameter of rebar (6, 6 mm; 10, 10 mm; 13, 13 mm)

Pitch of rebar (U, Unreinforced; 200, 200 mm; 400, 400 mm; 200/400, 200/400 mm)

Concrete strength (29, 29 N/mm^2; 39, 39 N/mm^2; 65, 65 N/mm^2)

Width of slab (300, 300 mm; 400, 400 mm; 500, 500 mm)

Length of stud (80, 80 mm; 100, 100 mm; 130, 130 mm)

Diameter of stud (16, 16 mm; 19, 19 mm; 22, 22 mm)

Table 2. Mix Proportion

W/C	s/a	Unit Materials Content [kg/m^3]				
		Water	Cement	Sand	Gravel	Admixture
51.0	47.1	179	351	814	950	4.21
41.5	45.5	170	410	775	960	4.71
35.9	45.8	172	479	755	902	4.79

Table 3. Material Properties: (a) concrete, (b) headed stud, (c) rebar, and (d) H-section steel.

(a)

W/C [%]	Compressive Strength [N/mm^2]	Tensile Strength [N/mm^2]	Modulus of Elasticity [N/mm^2]
51.0	29.1	3.6	20,111
41.5	38.7	4.2	24,051
35.9	64.8	5.7	33,877

(b)

Diameter [mm]	Length [mm]	Yield Stress [N/mm^2]	Ultimate Stress [N/mm^2]	Elongation [%]
16	130	411	473	33
19	130	391	486	25
22	80	398	461	25
	100	351	446	25
	130	384	464	27

(c)

Diameter [mm]	Yield Stress [N/mm^2]	Ultimate Stress [N/mm^2]	Elongation [%]
6	360	506	31
10	372	509	28
13	350	493	26

(d)

Yield Stress [N/mm^2]	Ultimate Stress [N/mm^2]	Elongation [%]
291	427	44

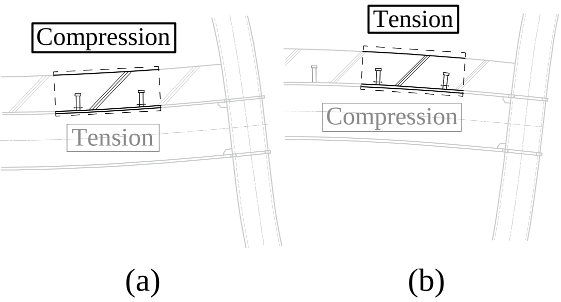

Fig. 1. Stress History of Concrete Slab: (a) positive bending and (b) negative bending

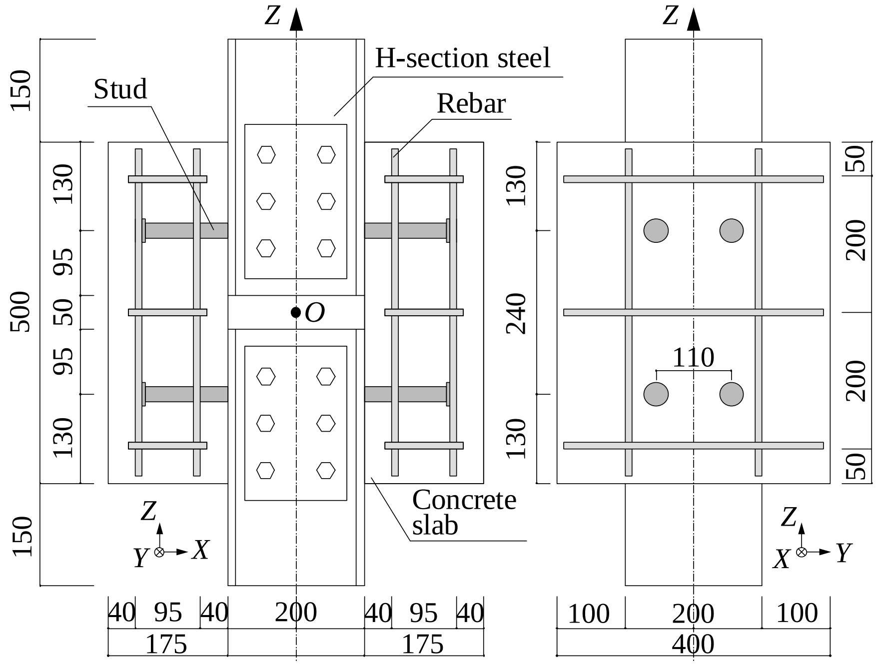

(a) (b)

Fig. 2. Component Model in Composite Structure (unit: mm): (a) side view and (b) front view.

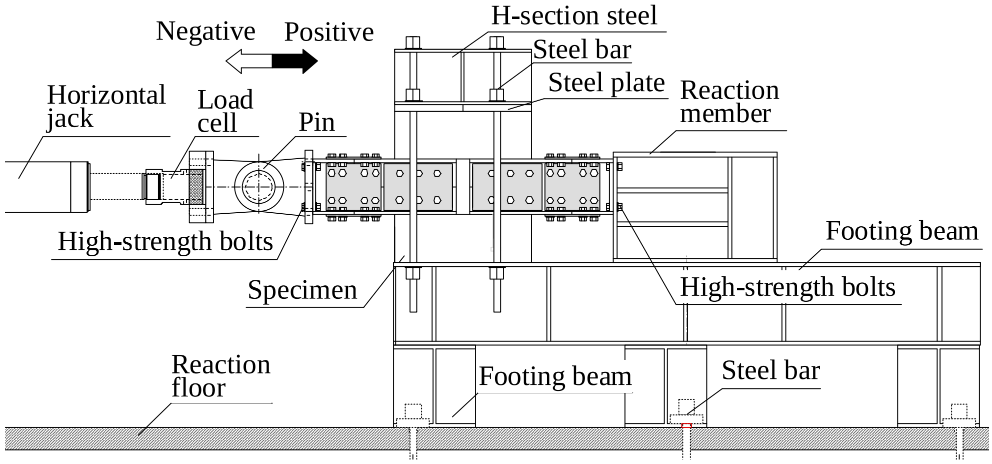

(a)

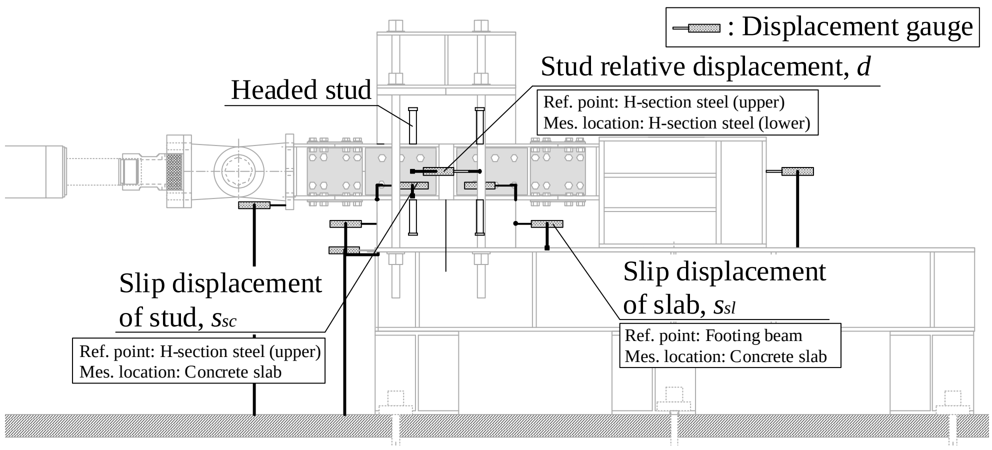

(b)

Fig. 3. Loading Frame (unit: mm): (a) setup of specimen and (b) installation of displacement gauges

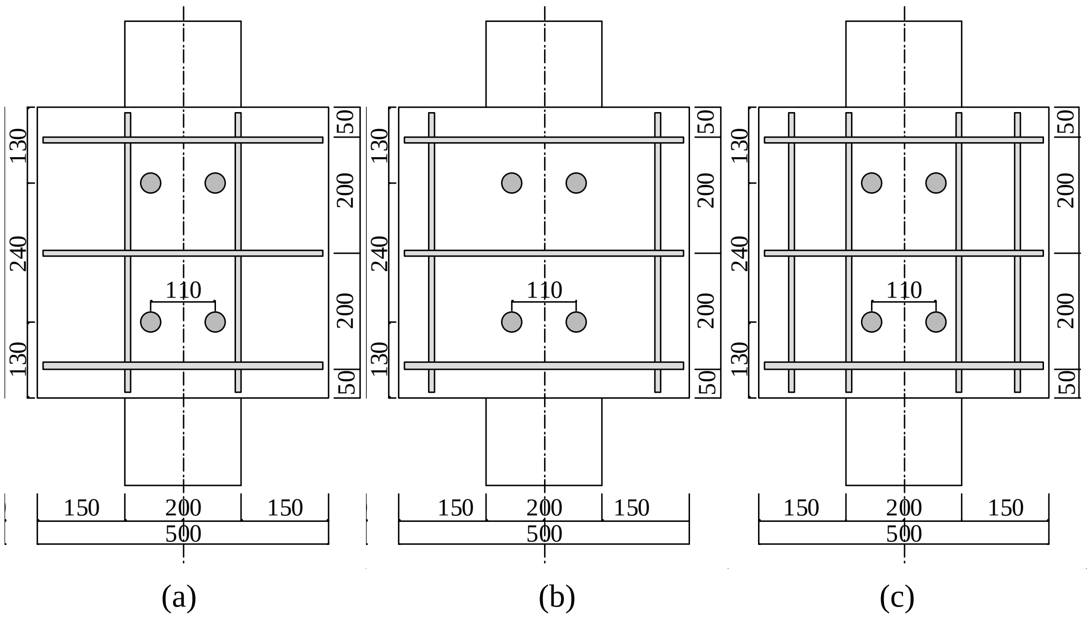

Fig. 4. Arrangement of Rebar (unit: mm): (a) No. 8, (b) No. 9, (c) No. 10.

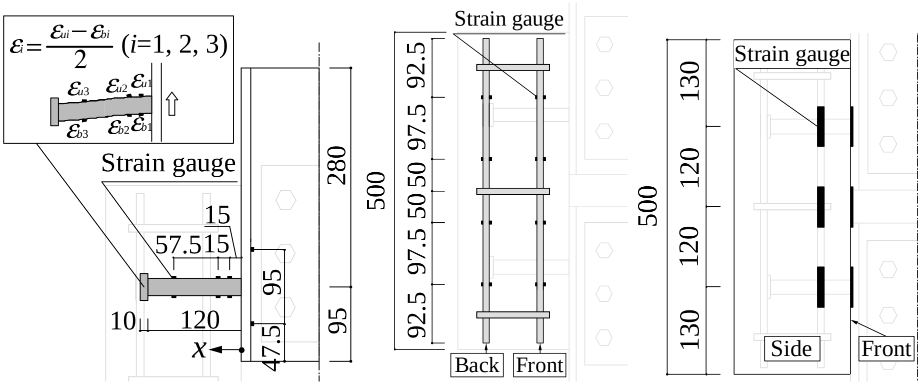

(a) (b) (c)

Fig. 5. Attachment of Strain Gauges (unit: mm): (a) stud and jig, (b) rebar, and (c) concrete slab.

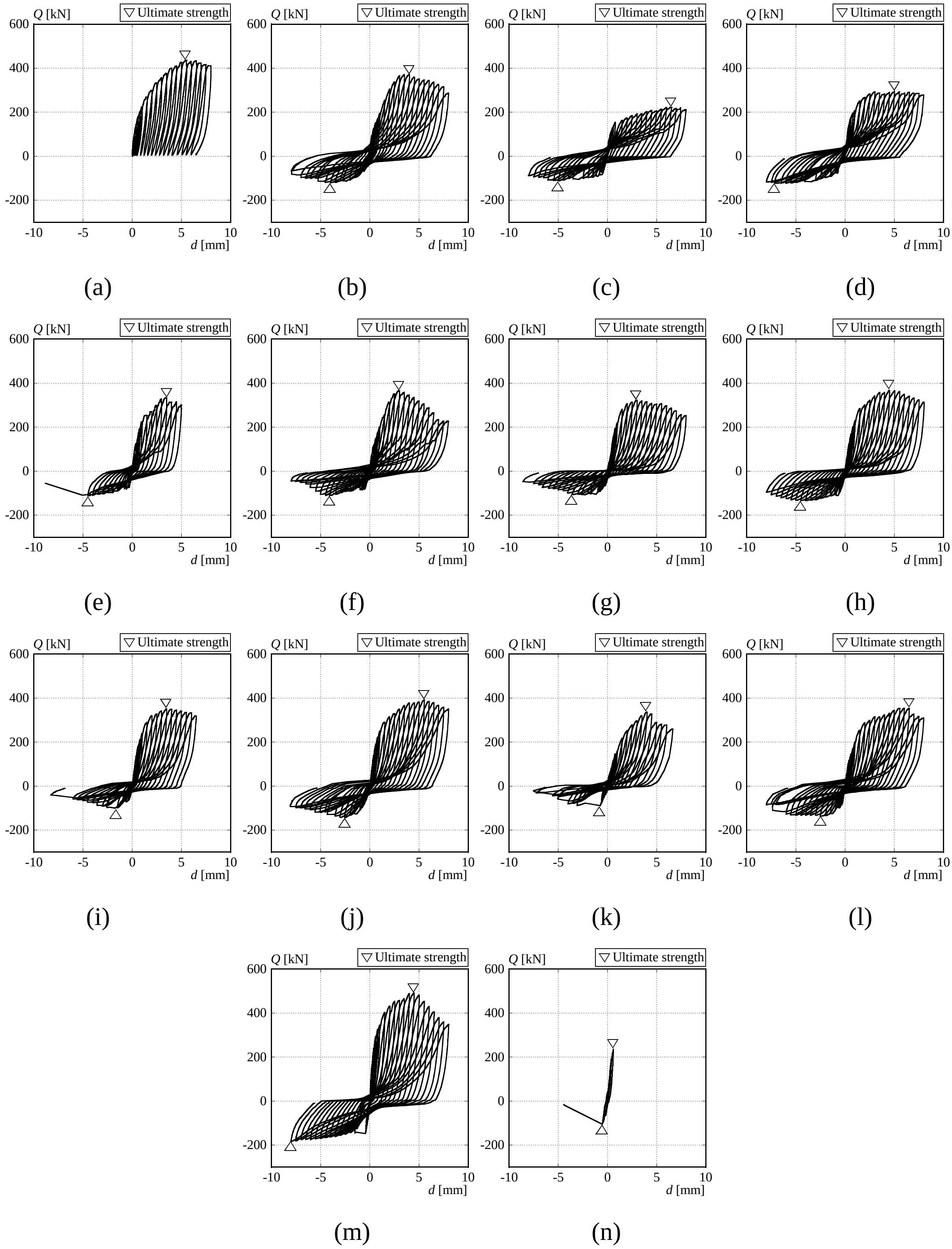

Fig. 6. Hysteresis Curves: (a) No. 1, (b) No. 2, (c) No. 3, (d) No. 4, (e) No. 5, (f) No. 6, (g) No. 7, (h) No. 8, (i) No. 9, (j) No. 10, (k) No. 11, (l) No. 12, (m) No. 13, and (n) No. 14.

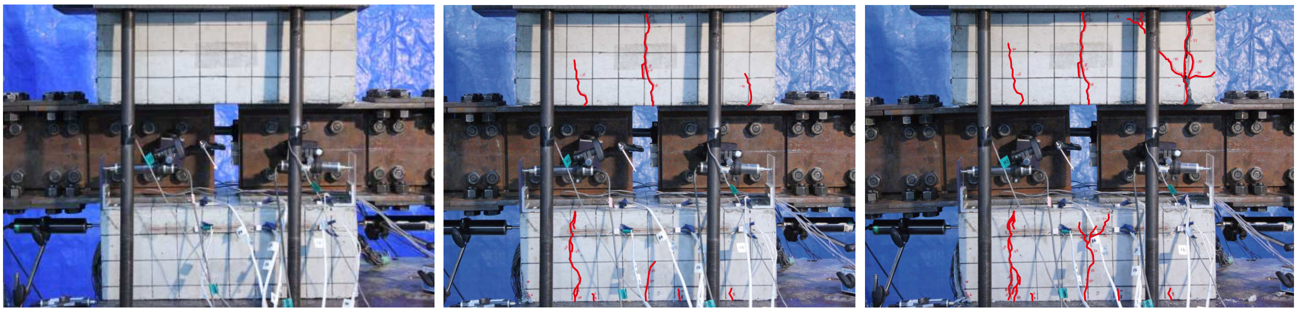

(a) (b) (c)

Fig. 7. Fracture Process: (a) d=0 mm, (b) d=-4.0 mm, and (c) d=-8.0 mm.

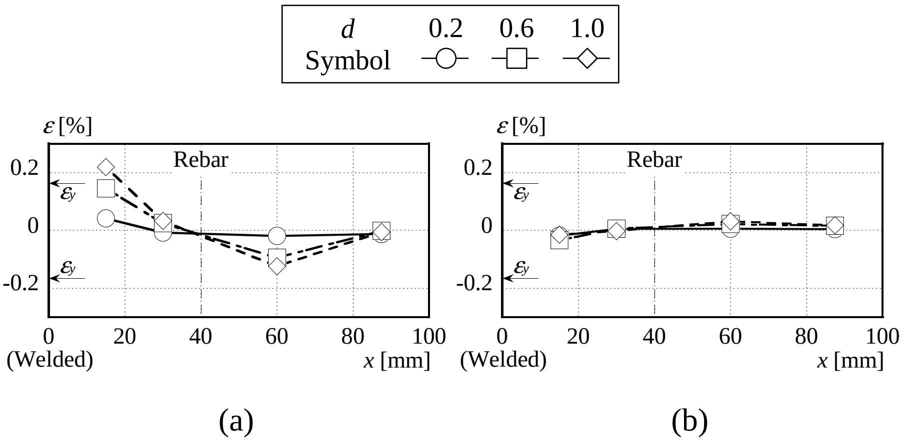

Fig. 8. Bending Strain of Stud: (a) positive and (b) negative.

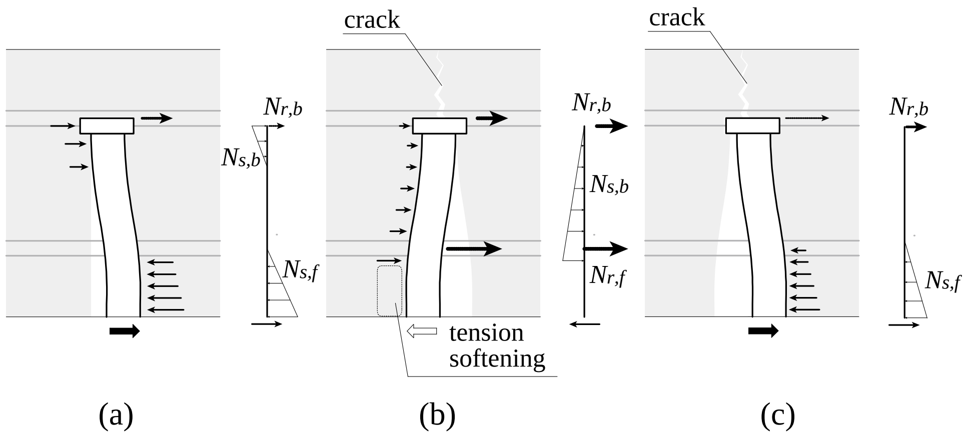

Fig. 9. Influence of Reversed Cyclic Loading: (a) first positive side loading, (b) following negative side loading, and (c) following positive side loading.

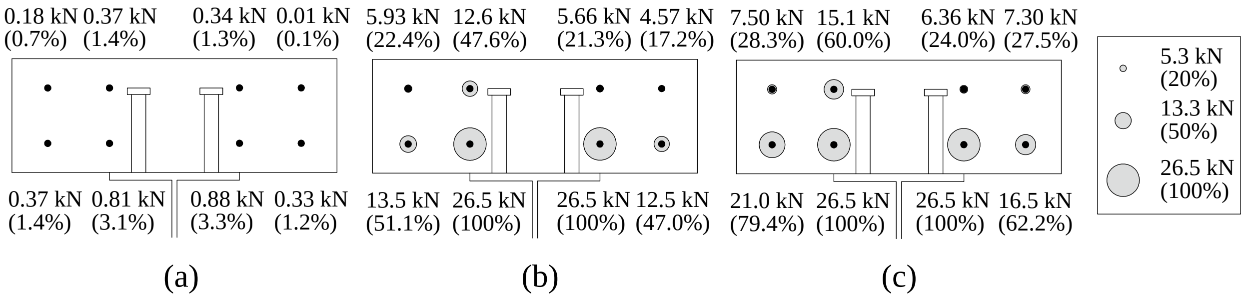

Fig. 10. Stress Distribution under Negative Side Loading (No. 10): (a) d=-1.0 mm, (b) d=-2.5 mm (ultimate shear strength), and (c) d=-4.0 mm.

No.	2	3	4	5	6	7	8	9	10	11	12	13	14
Symbol	●	○	●	■	◆	▲	▼	▽	▼	×	⊠	▢	+

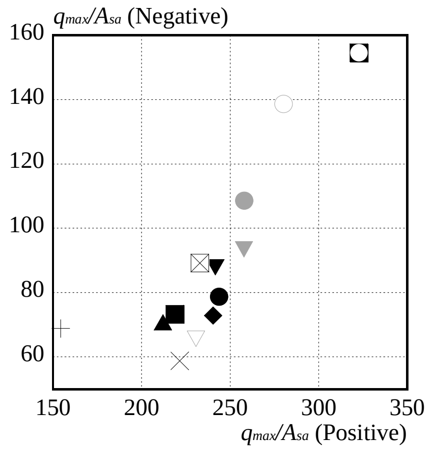

Fig. 11. Comparison of Ultimate Shear Strength of Positive and Negative Sides.

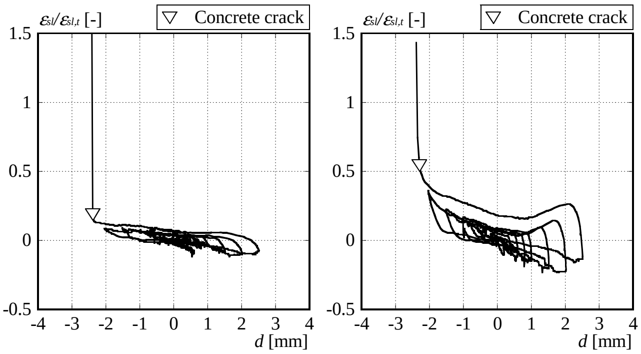

(a) (b)

Fig. 12. Strain of Concrete Slab: (a) side (left side, *Z*=120 mm) and (b) front (left side, *Z*=120 mm)

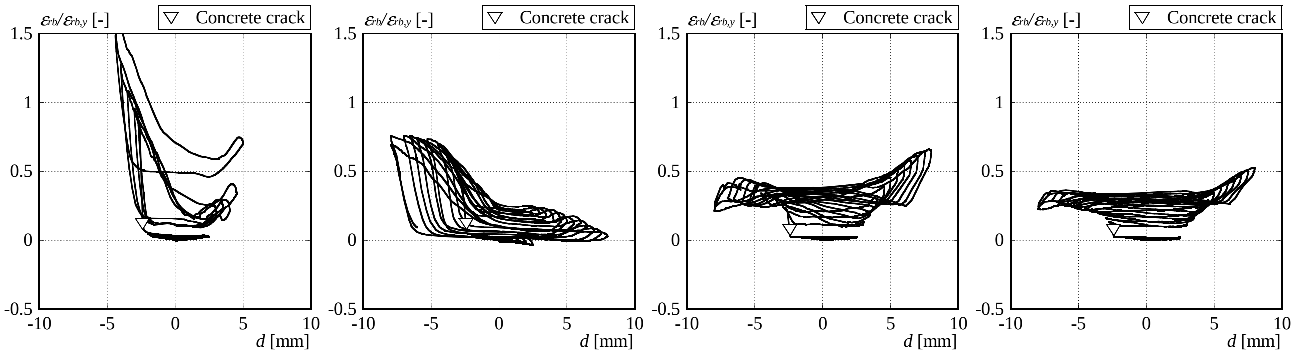

(a) (b) (c) (d)

Fig. 13. Strain of Rebar: (a) front (left side, *Z*=147.5 mm), (b) front (left side, *Z*=50 mm), (c) back (left side, *Z*=147.5 mm), and (d) back (left side, *Z*=50 mm).

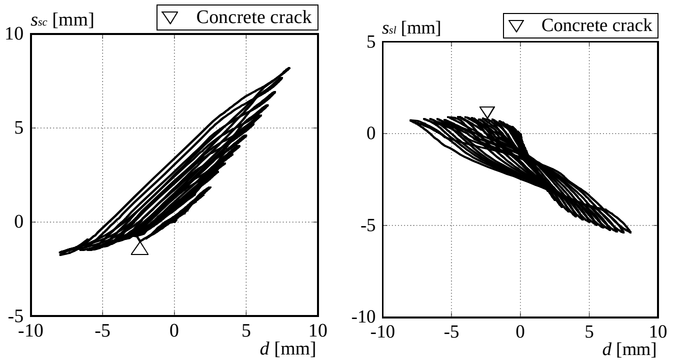

(a) (b)

Fig. 14. Slip Behavior: (a) headed stud and (b) concrete slab.

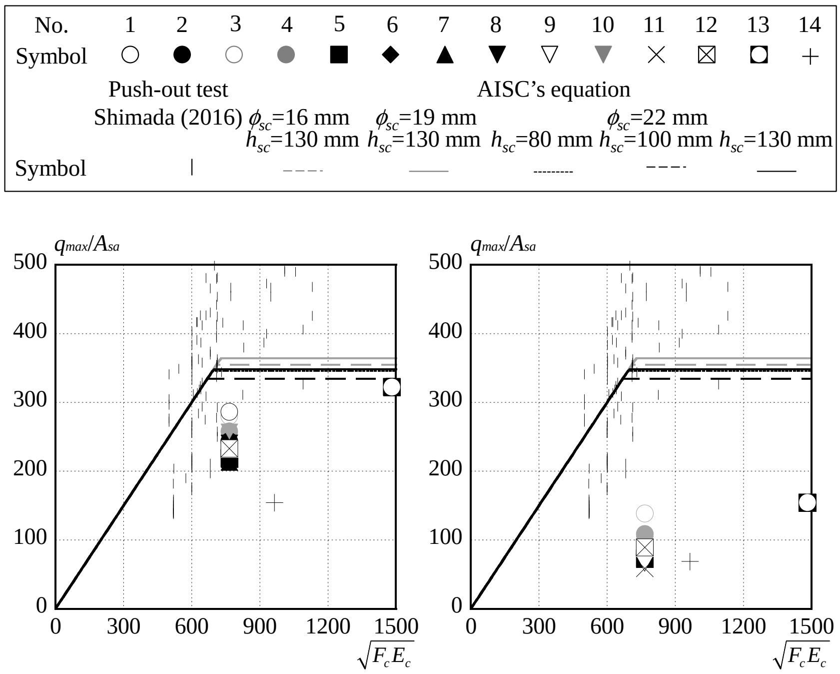

(a) (b)

Fig. 15. Comparison between Experimental Results and AISC's Equation: (a) positive and (b) negative.

No.	1	2	3	4	5	6	7	8	9	10	11	12	13	14
Symbol	○	●	○	●	■	◆	▲	▼	▽	▼	×	⊠	◘	+

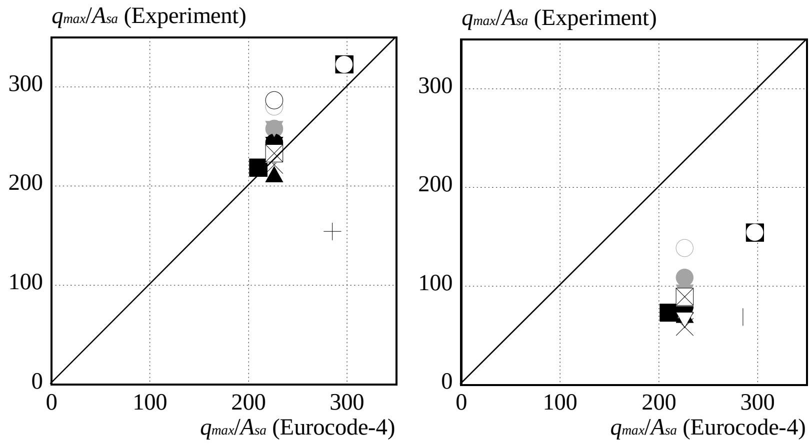

(a) (b)

Fig. 16. Comparison between Experimental Results and Eurocode-4’s Equation: (a) positive and (b) negative.

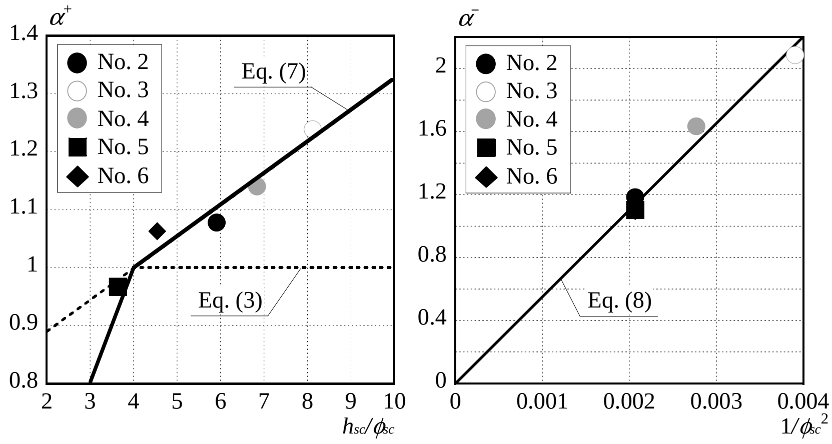

(a) (b)

Fig. 17. Coefficients α^+ and α^- arranged by h_{sc}/ϕ_{sc} and $1/\phi_{sc}{}^2$: (a) positive and (b) negative.

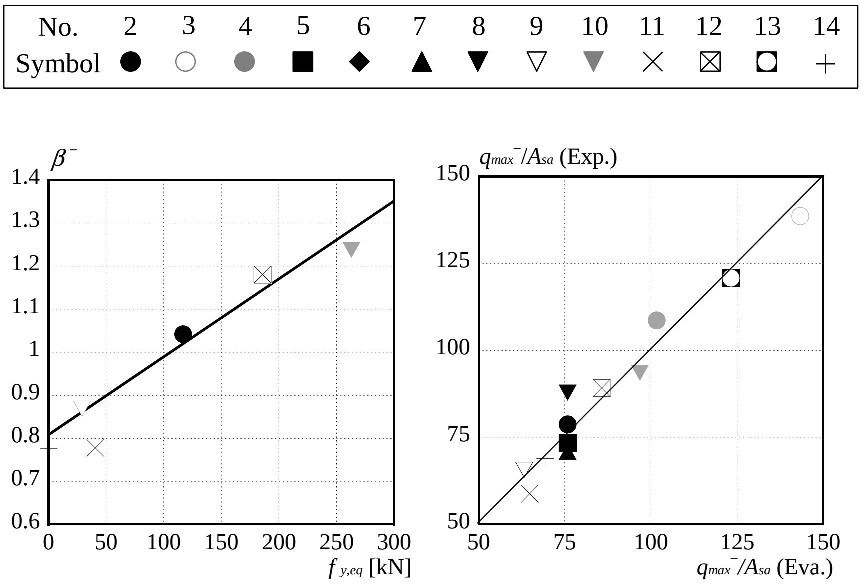

(a) (b)

Fig. 18. Evaluation of the ultimate shear strength in the negative side: (a) reduction factor and (b) comparison.

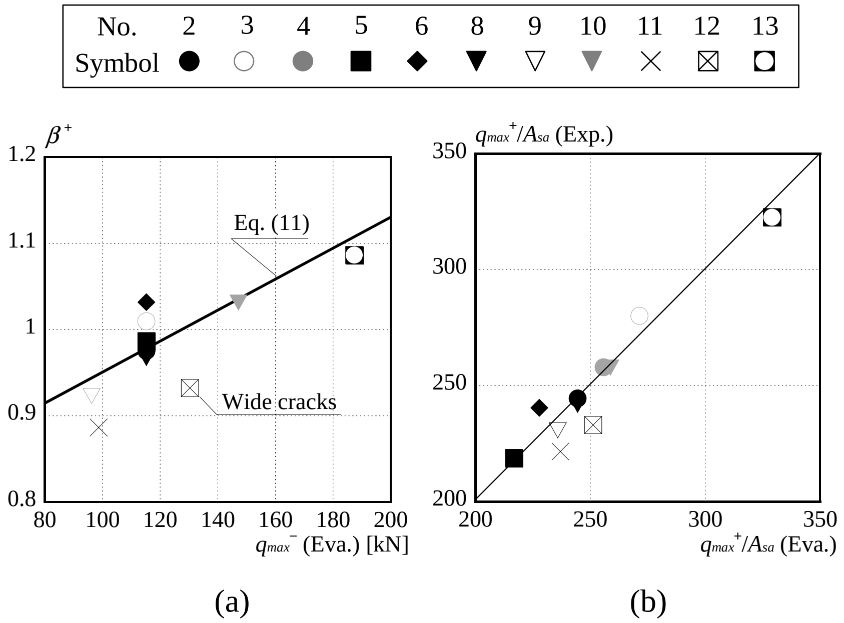

Fig. 19. Evaluation of Ultimate Shear Strength in Positive Side: (a) correction factor and (b) comparison.